minerals

MDPI

Article

Confirmation of Siderazot, $Fe_3N_{1.33}$, the Only Terrestrial Nitride Mineral

Sebastian Bette [1], Thomas Theye [2], Heinz-Jürgen Bernhardt [3], William P. Clark [2,4] and Rainer Niewa [2,*]

[1] Max-Planck-Institute for Solid State Research, Heisenbergstraße 1, 70569 Stuttgart, Germany; S.Bette@fkf.mpg.de
[2] Institute of Inorganic Chemistry, Universität Stuttgart, Pfaffenwaldring 55, 70569 Stuttgart, Germany; thomas.theye@imi.uni-stuttgart.de (T.T.); william.clark@cpfs.mpg.de (W.P.C.)
[3] Department of Geology, Mineralogy and Geophysics, Ruhr-Universität Bochum, Universitätsstraße 150, 44801 Bochum, Germany; heinz-juergen.bernhardt@rub.de
[4] Max-Planck-Institute for Chemical Physics of Solids, Nöthnitzer Straße 40, 01187 Dresden, Germany
* Correspondence: rainer.niewa@iac.uni-stuttgart.de

Abstract: Siderazot, the only terrestrial nitride mineral, was reported only once in 1876 to occur as coating on volcanic rocks in a fumarolic environment from Mt. Etna and, to date, has been neither confirmed nor structurally characterized. We have studied the holotype sample from the Natural History Museum, London, UK, originally collected by O. Silvestri in 1874, and present siderazot with ε-Fe_3N-type crystal structure and composition of $Fe_3N_{1.33(7)}$ according to crystal structure Rietveld refinements, in good agreement with electron microprobe analyses. Crystal structure data, chemical composition, and Raman and reflectance measurements are reported. Possible formation conditions are derived from composition and phase stability data according to synthetic samples.

Keywords: siderazot; silvestrite; Fe_3N; iron; nitride

Citation: Bette, S.; Theye, T.; Bernhardt, H.-J.; Clark, W.P.; Niewa, R. Confirmation of Siderazot, $Fe_3N_{1.33}$, the Only Terrestrial Nitride Mineral. *Minerals* **2021**, *11*, 290. https://doi.org/10.3390/min11030290

Academic Editor: Huifang Xu

Received: 24 February 2021
Accepted: 7 March 2021
Published: 11 March 2021

1. Introduction

Whereas almost all nitrogen in minerals is bound in the form of ammonium and nitrate salts, only few reports on nitride-containing minerals are available. A survey on these nitride minerals reveals that most are extra-terrestrial in origin, comprising the silicon minerals nierite, Si_3N_4, found in perchloric acid stable remains of the three common chondrite meteorites Inman, Adrar, and Tieschitz, and one enstatite meteorite (Indarch) as well as grains in the Murchison meteorite [1–8], and sinoite, Si_2N_2O, in chondrites [9–11] like the Jajh deh Kot Lalu meteorite, which fell on 2nd May 1926 in Sind Province, Pakistan [12]. Additionally, a few transition metal minerals, osbornite, TiN, from Bustee aubrite which fell in 1852 in Gorakhpur, Basti District, Uttar Pradesh, India, and from one meteorite of undefined locality in Russia [1,13], but further inferred to occur in other chondrites [14], carlsbergite, CrN, in meteorites Descubridora and Cape York (and about 70 more) [1,15,16], and roaldite, γ-Fe_4N, in meteorites Jerslev and Youndegin [17,18] were described. Exceptions from this extra-terrestrial origin are solely the mercury minerals gianellaite, $(Hg_2N)_2SO_4$ [19–22], kleinite, $Hg_2N((SO_4)_{0.25}Cl_{0.5})\cdot 0.5H_2O$, moesite, $Hg_2N(Cl,SO_4,MoO_4,CO_3)\cdot H_2O$ [1,23–25], and comancheite, $Hg_{55}N_{24}(OH,NH_2)_4(Cl,Br)_{34}$ [26]—derivatives of Millon's base—found first (and exploited from the mid-1880s until 1945) in Terlingua, Brewster Country, Texas, USA, and the rare siderazot (also called silvestrite, Fe_5N_2) [1,27,28] formed under the volcanic conditions of Mount Etna, Sicily.

The reason for the particular distribution of nitrogen and oxygen in the atmosphere and Earth's crust, as well as the predominately high oxidation state of nitrogen in minerals, can be found in the physical properties of nitrogen. The dissociation energy of the dinitrogen molecule and the electron affinity of nitrogen compared to the corresponding values for oxygen have to be considered. The dissociation energy of dinitrogen with $D(N_2)$ = +945 kJ/mol is about double that of dioxygen ($D(O_2)$ = +493 kJ/mol). While the

first electron affinity of both oxygen and nitrogen is negative, the sum of the first and second electron affinities of oxygen gives $\Sigma E_A(O)$ = +800 kJ/mol [29,30]. The corresponding values for the first, second, and third electron affinities of nitrogen sum up to about $\Sigma E_A(N)$ = +2300 kJ/mol [30–32], resulting in an unfavorable enthalpy of formation for metal nitrides compared to the corresponding metal oxides and explaining the formation of oxides rather than nitrides as thermodynamic stable products in atmospheres containing both gases, independent of temperature.

Several synthetic iron nitrides with a range of different compositions are known, comprising γ'-Fe_4N, ε-Fe_3N_{1+x}, and ζ-Fe_2N as stable phases occurring in the composition–temperature phase diagram, next to the metastable and high-pressure phases *bct* α'-Fe_8N and α''-$Fe_{16}N_2$ as an order variant thereof [33,34], and FeN in rock salt, in sphalerite, and in NiAs structure types [35–37]. In particular, γ'-Fe_4N and ε-Fe_3N_{1+x} play an important role in the industrial steel surface hardening process, improving hardness and tribological properties as well as corrosion and wear resistance of the work piece [38,39]. Furthermore, the ferromagnetic iron nitrides are the focus of research with magnetic data recording materials according to their tunable magnetic properties [40,41], while α'-Fe_8N and α''-$Fe_{16}N_2$ are considered as relevant rare-earth-free magnetic materials [42]. ε-Fe_3N_{1+x} stands out with a huge homogeneity range from about $Fe_3N_{0.75}$ to $Fe_3N_{1.5}$. ε-Fe_3N_{1+x} is known to be only a little susceptible to substitution by further transition metals [43–45] and for no significant incorporation of oxygen, but so-called carbonitrides form readily [39].

From those iron nitrides, only roaldite, γ'-Fe_4N, was detected to occur in meteoritic material as a late precipitate from kamacite, α-(Fe,Ni) [18]. None of these iron nitrides directly forms from iron or iron compounds and elemental nitrogen, except at elevated pressures combined with high temperatures [37,46,47]. ε-Fe_3N_{1+x} at ambient pressure can be synthetically obtained from elemental iron via treatment with pure ammonia at about 520 °C. The terrestrial mineral siderazot was only reported once in 1876 by O. Silvestri, who collected lava specimens released during the eruption of Etna at August 1874. He inferred the composition Fe_5N_2 from the reaction of the material with hydrogen, determining the amount of ammonia formed next to elemental iron [27,28]. This composition lies well within the homogeneity range of ε-Fe_3N_{1+x} (Fe_5N_2 = $Fe_3N_{1.2}$).

Iron nitrides are discussed as being of high significance in nitrogen storage in the deep Earth [48–53]. Relevant high-pressure phases in the Fe–N system were recently presented to occur via pressure-induced transition from pre-prepared iron nitrides or from reactions of elemental nitrogen with iron at elevated pressures and temperature [37,46,47,54]. Furthermore, Fe_2N, Fe_3N, and $Fe_9(C,N)_4$ were recently observed as inclusions in lower-mantle diamond from Rio Soriso, Brazil [55]. Nitrogen is suggested to show a rather siderophile character in the core's iron–nickel alloy, resulting in fairly high solubility [56]. Further, nitrides TiN and cubic BN were observed as inclusions in chromitite of a Tibetan ophiolite likely originating from the deep upper mantle or from the lower mantle [57].

The IMA (International Mineralogical Association) status of naturally occurring siderazot is "approved", "grandfathered" (first described prior to 1959), and "questionable" because no further data were published since the first description of the mineral by Silvestri in 1876 [27,28]. In this study, we present a detailed investigation of a historic mineral sample from the Natural History Museum in London that was collected more than 140 years ago. We identified siderazot in this sample and derived a phase composition of $Fe_3N_{1.33}$ from a microprobe and a crystal structure analysis by powder X-ray diffraction (PXRD). This is the first confirmation of a naturally occurring terrestrial iron nitride mineral.

2. Materials and Methods

2.1. Sample Origin

The studied sample was a minor part of a small specimen of vesicular lava of 1.23 g, measuring about 10 mm × 10 mm × 20 mm in size, present at the Natural History Museum in London, UK. According to the records of the museum, the specimen was purchased in 1890 as part of a collection of rocks and minerals originally belonging to G. F. Rodwell.

This particular sample is accompanied by a business card of Prof. Orazio Silvestri from the University of Catania, dated April 11th, 1880, giving a reference with best wishes to Prof. Rodwell. Furthermore, the sample ampule bears a label of Silvestri and the location of the sampling "la lava dell'Etna" together with the statement "raro", i.e., rare. Some more information can be found in a publication of G. F. Rodwell, who states that during the eruption of Etna in 1869, Von Waltershausen noticed silver-colored particles on some of the lava blocks, which were still hot and smoking. However, this material rapidly underwent change. Apparently, this specimen was not suitable for further analyses due to an insufficient quantity, but during the eruption of 1874, Silvestri collected a larger quantity of the substance and analyzed it. It shows a metallic luster similar to that of steel [27,28,58]. We thus have reason to believe that our studied sample is part of the original specimen collected by Silvestri in 1874. Furthermore, it appears that the sample stored in the museum was untouched ever since it was purchased.

2.2. Chemical Analysis

About 10 grains of siderazot were separated by hand-picking and embedded in Epoxy resin. These mounts were then ground and finally polished with 0.25 µm diamond suspension. Qualitative and quantitative measurements on siderazot were performed with an electron microprobe of the type Cameca SX100 at the Institute for Inorganic Chemistry, Stuttgart University, Stuttgart, Germany. This machine is equipped with a 5 WD spectrometer and a Thermo NSS EDS. The quantitatively measured elements comprise Fe, Na, O, and N. Standards for the quantitative measurements were natural pure albite (Na), hematite (O), and synthetic Fe_4N (synthesized and compositionally verified at the Max Planck Institute for Metals Research, renamed the Max Planck Institute for Intelligent Systems, Stuttgart, Germany). Fe was analyzed with a large LiF (LIF, $2d$ = 0.40267 nm) diffraction crystal, Na with thallium hydrogen phthalate (TAP, $2d$ = 2.5745 nm), O with PC0 (pseudocrystal, $2d$ = 4.5 nm), and N with PC2 (pseudocrystal, $2d$ = 9.5 nm). Experimental conditions were 15 kV and 40 nA. Detection limits with these conditions are ca. 500 ppm for Na, and 800 ppm for O. The surface of the polished section was not coated, but single grains of siderazot were electrically connected to the sample bearer with silver ink.

2.3. Reflectance Measurements

Measurements of the reflectance were performed in air with a Leitz Orthoplan on the sample polished grain mount that was used for the electron microprobe analyses. The microscope was optically connected to a Hamamatsu mini-spectrometer of the type C10083CA (Hamamatsu Photonics, Hamamatsu City, Japan). The standard used for the measurements is WTiC.

2.4. Raman Spectroscopy

A Raman spectrum of siderazot was acquired on the polished grain mount with a Horiba Xplora µ-Raman PLUS Microscope (Horiba, Tokyo, Japan), applying a laser with 532 nm. Successful measurements were performed with a 20 % attenuator applied to a 25 mW laser (of which about 60 % hit the sample). The final lens of the attached microscope was 50× for the measurement.

2.5. Powder X-ray Diffraction

A high-resolution laboratory powder X-ray diffraction (PXRD) pattern of the siderazot mineral sample was recorded on a Stoe-Stadi P powder diffractometer (STOE & Cie GmbH, Darmstadt, Germany) equipped with a triple array of Mythen 1 K detectors using Mo-$K_{\alpha 1}$ radiation from a primary Ge(111)-Johann-type monochromator in Debye–Scherrer geometry. As the amount of material was far too small for a conventional data collection, the sample preparation was carried out in a non-standard way (Figure 1). A small (only visible by using magnifying glasses or a microscope) aggregate of crystallites was glued with universal glue (Uhu Alleskleber, Uhu GmbH, Bühl, Germany) to the top of a 0.3 mm

borosilicate glass capillary (Hilgenberg glass No. 14). By using an X-ray camera (X-ray FDS 1.4 MPixel CCD (Photonic Science & Engineering Limited, Hastings, UK) with 8 mm active diagonal, Photonic Science), it was assured that the sample was situated within the X-ray beam. In order to improve the particle statistics, the capillary was positioned offset and rotated around the X-ray beam in a way that the siderazot crystallite aggregate always stayed in the center of the beam (Figure 1, yellow circle). Three measurements of 20 h scan time were accumulated for the data analysis.

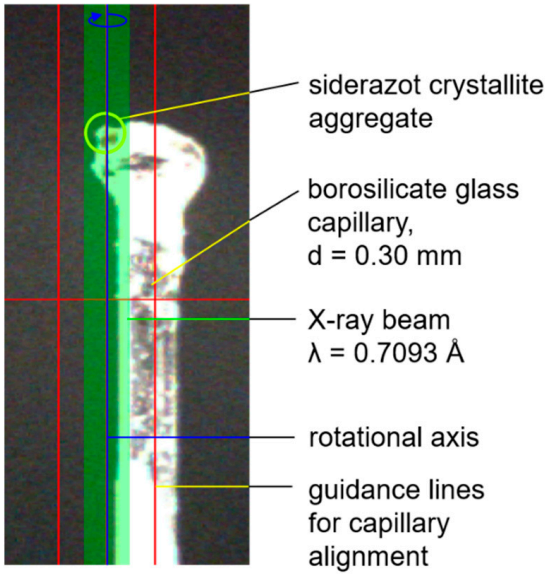

Figure 1. Experimental setup for collecting powder X-ray diffraction (PXRD) data of the siderazot mineral sample on a Stoe Stadi P powder diffractometer (Debye–Scherrer geometry) using Mo-$K_{\alpha 1}$ radiation.

2.6. Crystal Structure Refinements

The program TOPAS 6.0 [59] was used to analyze the PXRD data of the siderazot mineral sample. The instrumental profile was described by the fundamental parameter approach implemented in TOPAS [60] and the background was modeled by Chebychev polynomials of the 8th order. The humps in the background caused by the glue, the capillary, and by air scattering were modeled with broad Gaussian-type peaks. As a starting model for a fully weighted Rietveld refinement [61], the idealized hexagonal structure with space group $P6_322$ published by Jacobs et al. [62] was used. As the microprobe analysis (see Section 3.3) indicated an excess of nitrogen with respect to the ideal composition of Fe_3N, we inserted a second nitrogen atom on the 2*b* position as described by previous investigations [63,64] and refined its site occupancy. The refinement converged quickly. It should be noticed that the measured lattice parameters are in good agreement with the expected values for a phase composition of $Fe_3N_{1.33}$. The structural data were deposited in the CCDC database under the deposition number 2044590. These data can be obtained free of charge via http://www.ccdc.cam.ac.uk/conts/retrieving.html (deposited on 24 February 2021). The corresponding cif-file is additionally available online as Supplementary Materials.

3. Results and Discussion

Since the discovery of siderazot by Orazio Silvestri in 1876 in fumarole products at Etna, there has been no further scientific proof of this interesting mineral at all. Regardless, it has been introduced into various mineral databases, typically described as a thin coating on lava specimens, including the report of a Raman spectrum and a PXRD pattern with little information and unclear origin (https://rruff.info/Siderazot) (accessed on 22 August 2020). Additionally, there is an ongoing discussion on the identity of specimens referred to as siderazot in general. The reasons for this are the extreme rarity of the available samples and

possibly its limited long-term stability under ambient conditions, if only formed with small grain sizes. Even more surprising is the fact that Silvestri was able to determine the correct nitrogen content of 10 wt.% from a simple reaction with hydrogen and determination of the amount of formed ammonia [27,28]. This analysis nicely corresponds to our findings of 10.4 wt.% from microprobe analysis and 10.0 wt.% from Rietveld refinements of a PXRD pattern equaling a composition of $Fe_3N_{1.33(7)}$ (see below), also explaining the compositional assignment of $Fe_5N_2 \equiv Fe_3N_{1.2}$ (= 9.1 wt.% N) by the original author.

3.1. Sample Origin and Appearance

The studied sample was a minor part of a small specimen of vesicular lava obtained from the Natural History Museum in London, UK, apparently collected by O. Silvestri during the Etna eruption in 1874. For further information, please consult Section 2.1, Sample Origin.

The sample is not compact but consists of single grains with sizes of 0.05 to 1 mm. In addition to rock and mineral fragments, similarly sized pieces of laboratory glass and brush kemps were observed in the sample. It appears that the grains were collected by brushing off the surface of solidified lava. Most fragments have an angular, anhedral shape, but some euhedral feldspar crystals also occur. Clinopyroxene and volcanic glass were additionally identified by an EDS investigation on a grain mount. The presence of feldspar and clinopyroxene was also verified by X-ray examination of the bulk sample.

About 1% of the available sample consists of siderazot, as verified with the wavelength dispersive (WD) system of the electron microprobe. It forms small flakes with metallic, silvery luster. The grain size is rather uniform, ca. 0.1 to 0.2 mm in diameter. The surface of the flakes is not smooth but shows a granular structure. This is also visible in back-scattered electron images (Figure 2), where a pore structure can be recognized, consisting of numerous tiny spheres aggregated into larger grains. The size of single spheres is about 10 to 20 µm. The spheres are also visible in two-dimensional cross-sections through siderazot grains obtained from polished grain mounts (Figure 3). Here, roundish or slightly angular spheres of siderazot are well visible. A less porous type of siderazot also occurs (Figure 3c,d). A characteristic feature is the presence of vents in each sphere (Figure 2). Similar pore structures are frequently observed for synthetic iron nitride bulk materials as well as layers, where they are interpreted as degassing features at structural defects, due to excess nitrogen enrichments at interfaces and surfaces [65]. The hardness could not be measured because of the small grain size.

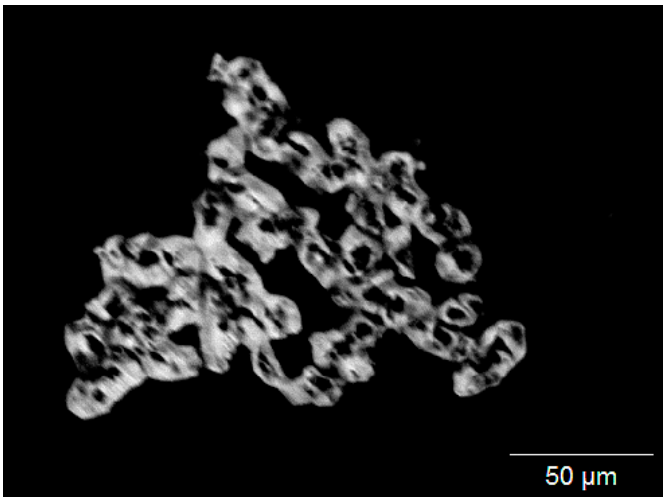

Figure 2. Aggregate of siderazot, BSE (backscattered electron) image of a grain mount (not polished). Note the granular surface structure. The sample appears to be composed of numerous small spheres with degassing vents.

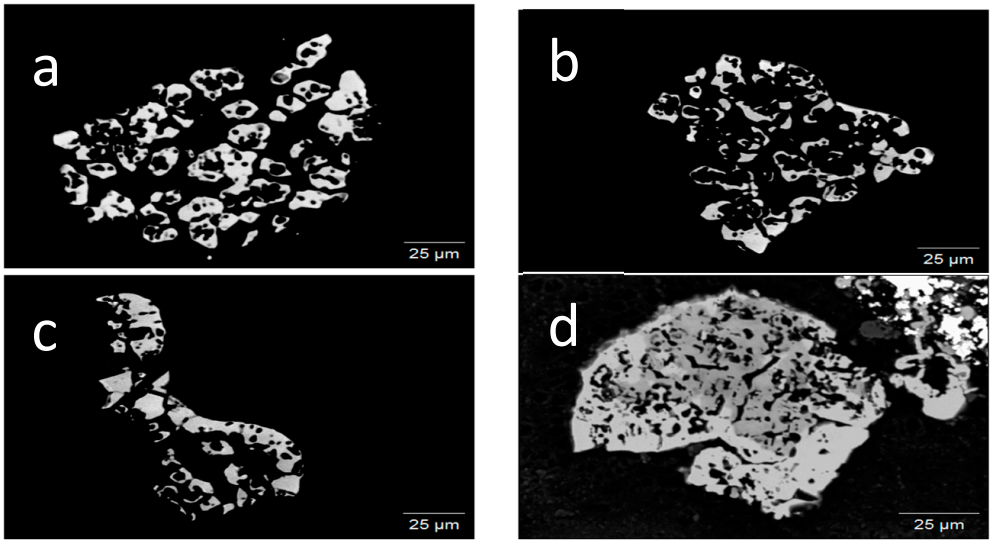

Figure 3. BSE images of a polished section, showing two-dimensional cross-sections through siderazot aggregates. Small spheres with central cavities (**a**–**c**) occur beside a less porous species (**c**,**d**). The aggregate in (**d**) contains a core of a dark gray Na-, Fe-, N-, and O-bearing phase, rimmed by the middle gray siderazot. The white phase in the upper right is baryte, associated with siderazot, and very dark gray K-feldspar.

3.2. Appearance in Reflected Light

The color of the mineral in reflected light is white to light gray with a yellowish tint. With crossed polarizers, it appears isotropic. No cleavage has been detected. The spectral reflectance is characterized by a constant increase with wavelength (Table 1, Figure 4). The calculated color values [66,67] are given in Table 2.

Table 1. Spectral reflectance of siderazot in air. The four wavelengths at 470, 546, 589, and 650 nm are interpolated. Unoriented sample.

λ/nm	R/%
400	46.7
420	47.2
440	48.2
460	49.0
470	49.3
480	49.6
500	50.4
520	51.1
540	51.8
546	52.0
560	52.5
580	53.2
589	53.5
600	53.8
620	54.5
640	55.2
650	55.5
660	55.8
680	56.5
700	57.3

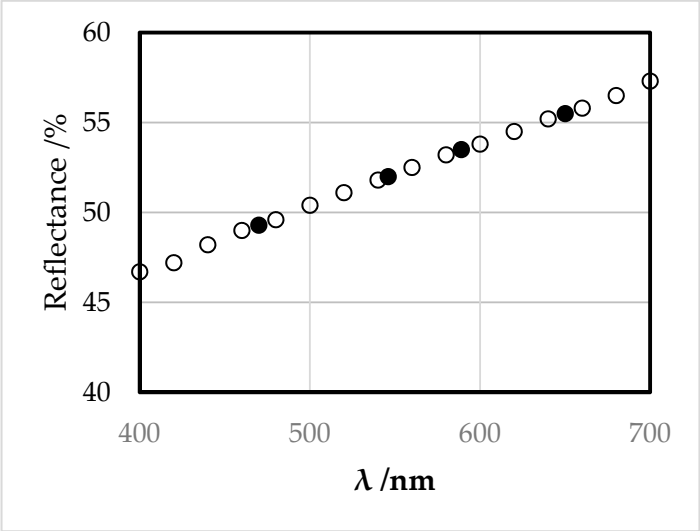

Figure 4. Reflectance of siderazot showing a constant increase with wavelength. Filled symbols are extrapolated wavelengths, open circles measured. Unoriented sample.

Table 2. Calculated color values of siderazot: x, y (chromatic coordinates), Y (luminance), λ_d (dominant wavelength), and P_e (excitation purity).

Illuminate	x	y	Y/%	λ_d/nm	P_e/%
C	0.3197	0.3245	52.3	579	4.8
A	0.4563	0.4091	52.8	588	7.2

3.3. Raman Spectroscopy

A Raman spectrum of siderazot was acquired by applying a green laser (532 nm) with low laser energy, since, at higher energy, it instantaneously converted to hematite. It appears that siderazot has a limited thermal stability at ambient atmospheric conditions.

Siderazot is a weak Raman scatterer. The spectrum is characterized by a single broad band at 540 cm^{-1} (Figure 5). This deviates from the siderazot spectrum in the Rruff.info database, where the mineral shows a broad band at ca. 500 cm^{-1}. However, these data were acquired from an undocumented sample of unclear origin. For synthetic ε-Fe_3N_{1+x}, we were unable to obtain any signal due to decomposition of this non-passivated material, as was earlier observed by different authors [68].

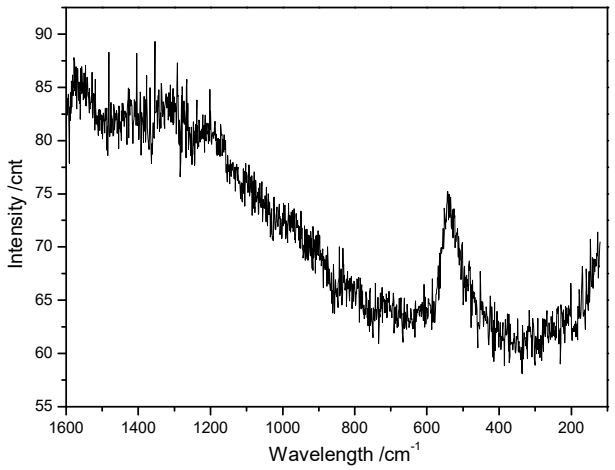

Figure 5. Raman spectrum of siderazot applying a green laser at 532 nm. No background correction, unoriented sample.

3.4. Chemical Analysis

Qualitative WD scans show that the composition of siderazot is rather simple. It exclusively contains Fe and N in addition to small amounts of O. Na only occurs in some restricted portions of siderazot aggregates (Figure 3d), together with elevated contents of oxygen. C is also visible in WD scans, but is attributed to contamination of the measurement spots by cracking products of oil released from the oil diffusion pump of the microprobe.

The quantitative measurements of siderazot reveal a very uniform chemical composition, with ca. 10.4 wt.% N and 88.7 wt.% Fe (Table 3). O is on average below 0.2 wt.%. It is suggested that the measured oxygen does not belong to siderazot, but that a surface layer is converted to hematite during the polishing process, similar to the case in the Raman experiments. Neglecting O and normalizing the atomic proportions to three iron atoms, an average (n = 24) formula of $Fe_3N_{1.4}$ results for the examined siderazot (Table 4), in good agreement with the composition of $Fe_3N_{1.33(7)}$ derived from structure Rietveld refinements presented in Section 3.4.

Table 3. Average elemental composition of siderazot grains from electron microprobe analysis averaged over 25 spots.

wt.%	n = 25	1σ	Min.	Max.
Fe	88.71	0.39	87.33	89.22
N	10.37	0.19	9.85	10.62
Na	<0.07	0.01	0.00	0.03
O	0.1	0.07	0.08	0.40
Total	99.30	0.40	98.12	99.87

Table 4. Average elemental composition of siderazot grains from electron microprobe analysis averaged over 25 spots as given in Table 1, normalized to a composition of Fe_3N_{1+x}.

	n = 25	1σ	Min.	Max.
Fe	3.000			
N	1.399	0.026	1.327	1.434
Na	0.025	0.009	0.009	0.047
O	0.000	0.001	0.000	0.002

In some of the siderazot aggregates, Na-bearing compositions occur (Table 5). They are characterized by a higher content of O, and a lower total, possibly indicating the presence of further elements. Additionally, these analyses are more heterogeneous than Na-poor siderazot. It is not clear whether this Na-bearing portion consists of an intimate mixture of different phases, or if it represents a distinct phase.

Table 5. Average elemental composition of Na-bearing siderazot grains from electron microprobe analysis averaged over 4 spots.

wt.%	n = 4	1σ	Min.	Max.
Fe	85.00	0.82	84.02	86.00
N	6.58	0.46	5.94	6.95
Na	1.99	0.76	1.05	2.90
O	1.68	0.37	1.18	2.05

Furthermore, microprobe analysis indicates no presence of further chemical elements within the grains of siderazot, except some Na-bearing domains, as discussed above. This fact can be understood from the chemical nature of ε-Fe_3N_{1+x}. This phase is known to be intolerant to substitution or uptake of other transition metals under low-pressure conditions, while at elevated pressures, solid solutions with Co, Ni, and Mn readily form. However, under ambient pressure conditions, these ternary phases are metastable with respect to decomposition into ternary γ′-phase nitrides and iron alloys [43]. Uptake of

oxygen is similarly prohibited due to the much higher thermodynamic stability of binary iron oxides, while carbon additions may lead to iron carbonitrides.

3.5. Crystal Structure Refinements

The crystal structure of the mineral phase was subjected to fully weighted Rietveld refinements [61] using the structure of synthetic ε-Fe_3N_{1+x} as a starting model. This provided an independent measure for the composition. For initial refinements, the idealized hexagonal structure for ε-Fe_3N in space group $P6_322$ was used [62]. Since the ε-type iron nitride is well known for a broad homogeneity range [69] and the microprobe analysis (Section 3.3) indicated an excess of nitrogen with respect to the ideal composition of Fe_3N, we inserted a second nitrogen atom in the 2*b* position as described by previous investigations [63,64] and refined its site occupancy. The refinements converged quickly, resulting in a composition of $Fe_3N_{1.33(7)}$. The resulting crystallographic data are listed in Tables 6 and 7. The graphical results of the final Rietveld refinement are presented in Figure 6. It should be noticed that the measured lattice parameters are in good agreement with the expected values (measured: a = 4.7527(1) Å, c = 4.4077(2) Å, expected: $a \approx 4.77$ Å, $c \approx 4.42$ Å [63]) for a phase composition of $Fe_3N_{1.33}$, according to relations for lattice parameters as a function of composition for synthetic samples. Selected interatomic distances and angles resulting from our crystal structure refinement are given in Table 8, which are in close agreement with distances obtained for synthetic samples [62,64].

Table 6. Selected crystallographic and Rietveld refinement data of siderazot.

Mineral Name	Siderazot
Sum formula	Fe_3N_{1+x} with x = 1.33
Molecular weight, g/mol	186.22
Temperature, K	295
Space group	$P6_322$
Z	2
a, Å	4.7527(1)
c, Å	4.4077(2)
V, Å^3	86.22(1)
ρ_{calc}, g·cm^{-3}	7.17
Wavelength, Å	0.7093
R-p, % [1]	1.28
R-wp, % [1]	1.60
R-F^2, % [1]	0.79
R-exp, % [1]	0.96
G.O.F. [1]	1.67
No. of variables	29

[1] G.O.F. (goodness of fit), *R-exp*, *R-p*, *R-wp*, and *R-F*^{2} as defined in TOPAS (Bruker AXS).

Table 7. Atomic coordinates of siderazot in ambient conditions.

Atom	Wyck.	Site	S.O.F. [1]	*x*	*y*	*z*	B_{eq}, Å^2
Fe	6*g*	.2.	1.00	0.322(1)	0	0	1.16(6)
N(1)	2*c*	3.2	1.00	1/3	2/3	1/4	B_{eq}(Fe) [2]
N(2)	2*b*	3.2	0.33(7)	0	0	1/4	B_{eq}(Fe) [2]

[1] Site occupation factor, [2] one global parameter for the B_{eq} of all sites was defined.

Table 8. Selected bond distances of siderazot in ambient conditions.

Atoms	Distance, Å	Atoms	Angle, deg
N(1)–Fe	6 × 1.951(8)	N(1)–Fe–N(1)	128.6(1)
N(2)–Fe	6 × 1.888(8)	N(2)–Fe–N(2)	71.5(1)
Fe–Fe	2 × 2.655(16)		
	4 × 2.684(5)		
	2 × 2.776(11)		
	4 × 2.790(8)		

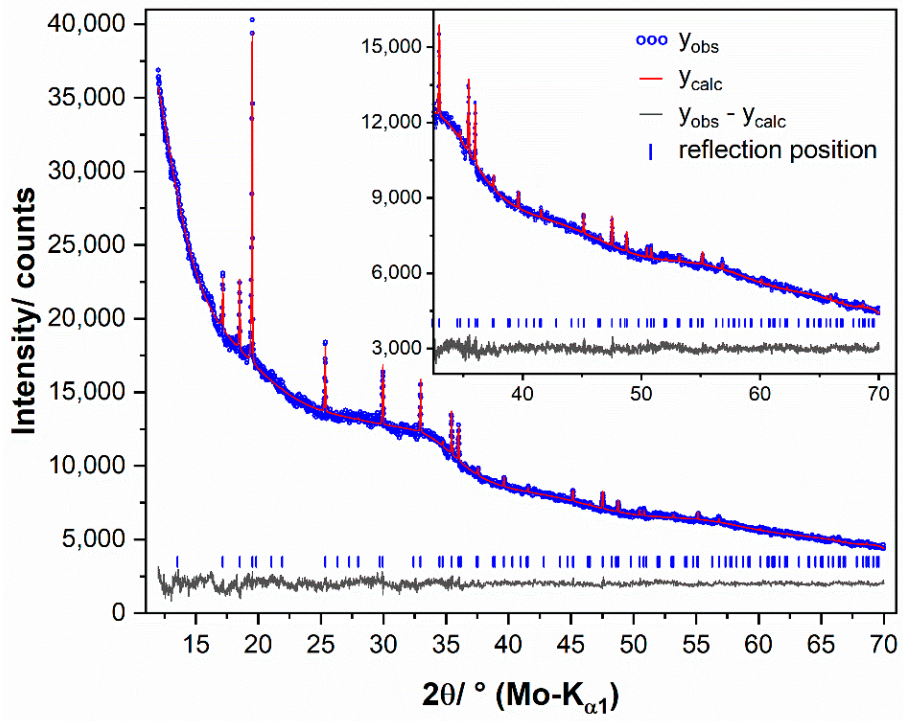

Figure 6. Graphical representation of the final Rietveld refinement of the mineral sample of siderazot. The high 2θ region starting at 32° is enlarged for clarity (inset).

3.6. Possible Formation Conditions

Initially, Rodwell noted for siderazot that it appears to be formed by the action of hydrochloric acid and ammonia on red-hot lava containing a large percentage of iron [58]. Synthesis of ε-type iron nitride phase (Fe_3N-type) with such a high nitrogen content from elemental iron is typically achieved at 520 °C in pure ammonia or ammonia–hydrogen mixtures [34,63]. Higher temperatures rather lead to lower nitrogen uptake, while larger concentrations of hydrogen favor the formation of cubic roaldite, γ'-Fe_4N. Ammonia and hydrogen are additionally known to reduce iron oxides to elemental iron under the formation of water even at much lower temperatures. This information can give us a clue to the formation conditions of siderazot. It appears that a fumarolic system is formed by the combination of main gaseous species (H_2O, CO_2, CO) with N_2, H_2, and NH_3, among others, which are known to be present deeper within the volcano, i.e., Vesuvius [70,71]. Such high-temperature fumaroles are typically rather short-lived. Ammonia likely is formed via the equilibrium Reaction (1), ammonia content is controlled by temperature and water and oxygen fugacities [72].

$$N_2 + 3\ H_2O \rightleftarrows 2\ NH_3 + 3/2\ O_2 \quad (1)$$

Since metallic iron cannot be expected as precursor phase of siderazot in a volcanic rock environment, magnetite, hematite, and ilmenite may be candidates instead, leading to the following simplified formation reactions (for different iron nitride compositions, accordingly):

$$2.66\ NH_3 + Fe_3O_4 \rightarrow Fe_3N_{1.4} + 4\ H_2O + 0.63\ N_2 \quad (2)$$

$$3\ NH_3 + 1.5\ Fe_2O_3 \rightarrow Fe_3N_{1.4} + 4.5\ H_2O + 0.8\ N_2 \quad (3)$$

$$2\ NH_3 + 3\ FeTiO_3 \rightarrow Fe_3N_{1.4} + 3\ TiO_2 + 3\ H_2O + 0.3\ N_2 \quad (4)$$

Particularly, magnetite is a common mineral in volcanic rocks from Mt. Etna [73] and may account for the formation of siderazot according to Reaction (2). Synthetic iron nitrides, in this respect, can be obtained from iron oxides via reduction–nitridation reactions in

one- or two-step processes [34,42,63]. Magnetite represents an early crystallized liquidus phase in these rocks [74], and a rather uniform grain size may be expected. This offers a good explanation for the flake-like grain shape and the limited grain size range of the examined siderazot sample, if it just forms in places where magnetite is exposed to a fumarolic environment on the surface of lava. In the above reactions, rather large volumes of gas are released, possibly contributing to the degassing feature described above.

Supplementary Materials: The following are available online at https://www.mdpi.com/2075-163X/11/3/290/s1, CIF: siderazot-mineral.

Author Contributions: Conceptualization, R.N.; validation, R.N.; formal analysis, S.B. and T.T.; investigation, W.P.C., S.B., T.T., and H.-J.B.; resources, R.N.; data curation, S.B. and T.T.; writing—original draft preparation, S.B., T.T., and R.N.; writing—review and editing, R.N.; project administration, R.N. All authors have read and agreed to the published version of the manuscript.

Funding: This research received no external funding.

Data Availability Statement: The crystal structure data were deposited in the CCDC database under the deposition number 2044590. These data can be obtained free of charge via http://www.ccdc.cam.ac.uk/conts/retrieving.html (accessed on 24 February 2021).

Acknowledgments: We would like to thank Mike Rumsey (Principal Curator, Minerals and Senior Curator in Charge) from the Natural History Museum in London for sample loan MIN2019-92 and particularly for his enthusiastic commitment, even more under the difficult conditions of the COVID-19 pandemic.

Conflicts of Interest: The authors declare no conflict of interest.

References

1. Anthony, J.; Bideaux, R.; Bladh, K.; Nichols, M. *Halides, Hydroxides, Oxides. Handbook of Mineralogy*; Mineral Data Publishing: Tuscon, AZ, USA, 1997; Volume 3.
2. Lee, M.R.; Russel, S.S.; Arden, J.W.; Pillinger, C.T. Nierite (Si_3N_4), a new mineral from ordinary and enstatite chondrites. *Meteorit. Planet. Sci.* **1995**, *30*, 387–398. [CrossRef]
3. Nittler, L.N.; Hoppe, P.; Alexander, C.M.O.'D.; Amari, S.; Eberhardt, P.; Gao, X.; Lewis, R.S.; Strebel, R.; Walker, R.M.; Zinner, E. Silicon nitride from supernovae. *Astrophys. J. Lett.* **1995**, *453*, L25–L28. [CrossRef]
4. Nittler, L.R. Presolar stardust in meteroites: Recent advances and scientific frontiers. *Earth Planet. Sci. Lett.* **2003**, *209*, 259–273. [CrossRef]
5. Alexander, C.M.O.'D. Presolar SiC in chondrites: How variable and how many sources? *Geochim. Cosmochim. Acta* **1993**, *57*, 2869–2888. [CrossRef]
6. Alexander, C.M.O.'D.; Swan, P.D.; Prombo, P.A. Occurrence and implications of silican nitride in enstantite chondrites. *Meteoritics* **1994**, *29*, 79–85. [CrossRef]
7. Stone, J.; Hutcheon, I.D.; Epstein, S.; Wasserburg, G.J. Correlated Si isotope anomalies and large ^{13}C enrichments in a family of exotic SiC grains. *Earth Planet. Sci. Lett.* **1991**, *107*, 570–581. [CrossRef]
8. Stone, J.; Hutcheon, I.D.; Epstein, S.; Wasserburg, G.J. Silicon, carbon and nitrogen isotopic studies of silicon carbide in carbonaceous and entstantite chondrites. In *Stable Isotope Geochemistry: A Tribute to Samuel Epstein*; Taylor, H.P., O'Neil, J.R., Kaplan, I.R., Eds.; Special Publication 3; The Geochemical Society: San Antonio, TX, USA, 1991; pp. 487–504.
9. Lacroix, A. Matériaux sur les météorites pierreuses; 1. Identitéde composition des météorites de Pillistfer (1863) et de Hvittis (1901). *Bull. Soc. Fr. Miner.* **1905**, *28*, 70–76.
10. Keil, K.; Andersen, C.A. Occurrences of sinoite, Si_2N_2O, in meteorites. *Nature* **1965**, *207*, 745. [CrossRef]
11. Rubin, A.E. Sinoite (Si_2N_2O): Crystallization from EL chondrite impact melts. *Am. Miner.* **1997**, *82*, 1001–1006. [CrossRef]
12. Andersen, C.A.; Keil, K.; Mason, B. Silicon oxynitride: A meteoritic mineral. *Science* **1964**, *146*, 256–257. [CrossRef]
13. Bannister, F.A. Osbornite, meteoritic titanium nitride. *Miner. Mag.* **1941**, *36*, 36–44. [CrossRef]
14. Grady, M.M.; Wrigth, I.P.; Carr, L.; Pillinger, C.T. Compositional differences in enstatite chondrites based on carbon and nitrogen stable isotope measurements. Geochim. *Cosmochim. Acta* **1986**, *50*, 2799–2813. [CrossRef]
15. Fleischer, M. New Mineral Names. *Am. Miner.* **1972**, *57*, 1311.
16. Buchwald, V.F.; Scott, E.R.D. First nitride (CrN) in iron meteorites. *Nat. Phys. Sci.* **1971**, *233*, 113–114. [CrossRef]
17. Cabri, L.J.; Fleischer, M.; Pabst, A. New Mineral Names. *Am. Miner.* **1981**, *66*, 1003–1099.
18. Buchwald, V.F.; Nielsen, H.P. Roaldite, a new nitride in iron meteorites. *Lunar Planet. Sci.* **1981**, *12*, 112–114.
19. Tunell, G.; Fahey, J.J.; Daugherty, F.W.; Gibbs, G.V. Gianellaite, a new mercury mineral. *Neues Jahrb. Miner. Monatsh.* **1977**, 119–131.
20. Fleischer, M.; Pabst, A.; Mandarino, J.A.; Chao, G.Y. New Mineral Names. *Am. Miner.* **1977**, *62*, 1057–1061.
21. Airoldi, R.; Magnano, G. Sulla struttura del sulfato (di)mercurioammonico. *Rass. Chim.* **1967**, *5*, 181–189.

22. Cooper, M.A.; Abdu, Y.A.; Hawthorne, F.C.; Kampf, A.R. The crystal structure of gianellaite, $[(NHg_2)_2](SO_4)(H_2O)_x$, a framework of ($NHg_4$) tetrahedra with ordered (SO_4) groups in the interstices. *Miner. Mag.* **2016**, *80*, 869–875. [CrossRef]
23. Foord, E.E.; Mills, B.A. Biaxiality in 'isomeric' and 'dimeric' crystals. *Am. Miner.* **1978**, *63*, 316–325.
24. Giester, G.; Mikenda, W.; Pertlik, F. Kleinite from Terlingua, Brewster County, Texas: Investigations by single crystal X-ray diffraction, and vibrational spectroscopy. *Neues Jahrb. Miner. Monatsh.* **1996**, *2*, 49–56.
25. Sachs, A. Der Kleinit, ein hexagonales Quecksilberoxychlorid von Terlingua in Texas. In *Sitzungsberichte der Königlich Preussischen Akademie der Wissenschaften*; Verlag der königlichen Akademie der Wissenschaften: Berlin, Germany, 1905; Zweiter Halbband; pp. 1091–1094.
26. Cooper, M.A.; Abdu, Y.A.; Hawthorne, F.C.; Kampf, A.R. The crystal structure of comancheite, $Hg^{2+}{}_{55}N^{3-}{}_{24}(OH,NH_2)_4(Cl,Br)_{34}$, and crystal-chemical and spectroscopic discrimination of N^{3-} and O^{2-} anions in Hg^{2+} compounds. *Miner. Mag.* **2013**, *77*, 3217–3237. [CrossRef]
27. Silvestri, O. Das Vorkommen des Stickstoffeisens unter den Fumarolen-Producten des Aetna und künstliche Darstellung dieser Verbindung. *Poggendorfs Ann. Phys. Chem.* **1876**, *157*, 165–172. [CrossRef]
28. Silvestri, O. La scombinazione chimica (dissociazione) applicata alla interpetrazione di alcuni fenomeni vulcanici; sintesi e analisi di un nuovo minerale trovato sull'Etna e di origine comune nei vulcani. *Atti Accad. Gioenia Sci. Nat.* **1876**, *10*, 17–27.
29. Huggins, M.L.; Sakamoto, Y. Lattice Energies and Other Properties of Crystals of Alkaline Earth Chalcogenides. *J. Phys. Soc. Jpn.* **1957**, *12*, 241–251. [CrossRef]
30. Ladd, M.F.C.; Lee, W.H. Lattice energies and related topics. *Prog. Solid State Chem.* **1967**, *3*, 265–288. [CrossRef]
31. Baughan, E.C. The Repulsion Energies in Ionic Compounds. *Trans. Faraday Soc.* **1959**, *55*, 736–752. [CrossRef]
32. Jack, K.H. The iron-nitrogen system: The preparation and the crystal structures of nitrogen-austenite (γ) and nitrogen-martensite (α'). *Proc. R. Soc. Lond. Ser. A* **1951**, *208*, 200–215. [CrossRef]
33. Jack, K.H. The occurrence and the crystal structure of α''-iron nitride; a new type of interstitial alloy formed during the tempering of nitrogen-martensite. *Proc. R. Soc. Lond. Ser. A* **1951**, *208*, 216–224. [CrossRef]
34. Widenmeyer, M.; Hansen, T.C.; Niewa, R. Formation and Decomposition of Metastable α''-$Fe_{16}N_2$ from in situ Powder Neutron Diffraction and Thermal Analysis. *Z. Anorg. Allg. Chem.* **2013**, *639*, 2851–2859. [CrossRef]
35. Suzuki, K.; Morita, H.; Kaneko, T.; Yoshida, H.; Fujimori, H. Crystal structure and magnetic properties of the compound FeN. *J. Alloys Compds.* **1993**, *201*, 11–16. [CrossRef]
36. Suzuki, K.; Yamaguchi, Y.; Kaneko, T.; Yoshida, H.; Obi, Y.; Fujimori, H.; Morita, H. Neutron Diffraction Studies of the Compounds MnN and FeN. *J. Phys. Soc. Jpn.* **2001**, *70*, 1084–1089. [CrossRef]
37. Clark, W.P.; Steinberg, S.; Dronskowski, R.; McCammon, C.; Kupenko, I.; Bykov, M.; Dubrovinsky, L.; Akselrud, L.G.; Schwarz, U.; Niewa, R. High-pressure NiAs-Type Modification of FeN. *Angew. Chem. Int. Ed.* **2017**, *56*, 7302–7306. [CrossRef] [PubMed]
38. Fry, A. Stickstoff im Eisen, Stahl und Sonderstahl. Ein neues Oberflächenhärtungsverfahren. *Stahl Eisen* **1923**, *43*, 1271–1279.
39. Prenosil, B. Einige neue Erkenntnisse über das Gefüge von um 600 °C in der Gasatmosphäre carbonitridierten Schichten. *Härt.-Technol. Mitt.* **1973**, *28*, 157–164.
40. Andriamandroso, D.; Fefilatiev, L.; Demazeau, G.; Fournès, L.; Purchard, M. Mossbauer resonance studies on Sn substituted Fe_4N. *Mater. Res. Bull.* **1984**, *19*, 1187–1194. [CrossRef]
41. Kim, T.K.; Takahashi, M. New magnetic materials having ultrahigh magnetic moment. *Appl. Phys. Lett.* **1972**, *20*, 492–494. [CrossRef]
42. Dirba, I.; Komissinskiy, P.; Gutfleisch, O.; Alff, L. Increased magnetic moment induced by lattice expansion from α-Fe to α'-Fe_8N. *J. Appl. Phys.* **2015**, *117*, 173911. [CrossRef]
43. Guo, K.; Rau, D.; Toffoletti, L.; Müller, C.; Burkhardt, U.; Schnelle, W.; Niewa, R.; Schwarz, U. The ternary metastable nitrides Fe_2TMN (*TM* = Co, Ni): High-pressure high-temperature synthesis, crystal structure, thermal stability and magnetic properties. *Chem. Mater.* **2012**, *24*, 4600–4606. [CrossRef]
44. Guo, K.; Rau, D.; Schnelle, W.; Burkhardt, U.; Niewa, R.; Schwarz, U. High-Pressure–High-Temperature Synthesis of ε-$Fe_2IrN_{0.24}$. *Z. Anorg. Allg. Chem.* **2014**, *640*, 814–818. [CrossRef]
45. Schwarz, U.; Guo, K.; Clark, W.P.; Burkhardt, U.; Bobnar, M.; Castillo, R.; Akselrud, L.; Niewa, R. Ferromagnetic ε-Fe_2MnN: High-pressure synthesis, hardness and magnetic properties. *Materials* **2019**, *12*, 1993. [CrossRef] [PubMed]
46. Bykov, M.; Bykova, E.; Aprilis, G.; Glazyrin, K.; Koemets, E.; Chuvashova, I.; Kupenko, I.; McCammon, C.; Mezouar, M.; Prakapenka, V.; et al. Fe–N system at high pressure reveals a compound featuring polymeric nitrogen chains. *Nat. Commun.* **2018**, *9*, 2756. [CrossRef] [PubMed]
47. Hasegawa, M.; Yagi, T. Synthesis of Metal Nitride Using Nitrogen Fluid under High Pressure and High Temperature—Synthesis and Physical Property. *Rev. High Press. Sci. Technol.* **2004**, *14*, 253–259. [CrossRef]
48. Mysen, B. Nitrogen in the Earth: Abundance and transport. *Prog. Earth Planetary Sci.* **2019**, *6*, 38. [CrossRef]
49. Bajgain, S.K.; Mookherjee, M.; Dasgupta, R.; Ghosh, D.B.; Karki, B.B. Nitrogen Content in the Earth's Outer Core. *Geophys. Res. Lett.* **2019**, *46*, 89–98. [CrossRef]
50. Liu, J.; Dorfman, S.M.; Lv, M.; Li, J.; Zhu, F.; Kono, Y. Loss of immiscible nitrogen from metallic melt explains Earth's missing nitrogen. *Geochem. Perp. Lett.* **2019**, *11*, 18–22. [CrossRef]
51. Adler, J.F.; Williams, Q. A high-pressure X-ray diffraction studies of iron nitrides: Implication for Earth's core. *J. Geophys. Res.* **2005**, *110*, B011203. [CrossRef]

52. Roskosz, M.; Bouhifd, M.A.; Jephcoat, A.P.; Marty, B.; Mysen, B.O. Nitrogen solubility in molten metal and silicate at high pressure and temperature. *Geochim. Cosmochim. Acta* **2013**, *121*, 15–28. [CrossRef]
53. Litasov, K.D.; Shatskiy, A.; Ponomarev, D.S.; Gavryushkin, P.N. Equations of state of iron nitrides ε-Fe_3N_x and γ-Fe_4N_y to 30 GPa and 1200 K and implication for nitrogen in the Earth's core. *J. Geophys. Res. Solid Earth* **2017**, *122*, 3574–3584. [CrossRef]
54. Minobe, S.; Nakajima, Y.; Hirose, K.; Ohishi, Y. Stability and compressibility of a new iron-nitride β-Fe_7N_3 to core pressures. *Geophys. Res. Lett.* **2015**, *42*, 5206–5211. [CrossRef]
55. Kaminsky, F.; Wirth, R. Nitrides and carbonitrides from the lowermost mantle and their importance in the search for Earth's "lost" nitrogen. *Amer. Miner.* **2017**, *102*, 1667. [CrossRef]
56. Miyazaki, A.; Hiyagon, H.; Sugiura, N.; Hirose, K.; Takahashi, E. Solubilities of nitrogen and noble gases in silicate melts under various oxygen fugacities: Implications for the origin and degassing history of nitrogen and noble gases in the Earth. *Geochim. Cosmochim. Acta* **2004**, *68*, 387–401. [CrossRef]
57. Dobrzhinetskaya, L.F.; Wirth, R.; Yang, J.; Hutcheon, I.D.; Weber, P.K.; Green, H.W. High-pressure highly reduced nitrides and oxidesfrom chromitite of a Tibetan ophiolite. *Proc. Natl. Acad. Sci. USA* **2009**, *106*, 19233–19238. [CrossRef]
58. Rodwell, G.F. *Etna: A History of the Mountain and Its Eruptions*; Cambridge University Press: London, UK, 1878; p. 134.
59. Coelho, A.A. TOPAS and TOPAS-Academic: An optimization program integrating computer algebra and crystallographic objects written in C plus. *J. Appl. Crystallogr.* **2018**, *51*, 210–218. [CrossRef]
60. Cheary, R.W.; Coelho, A.A.; Cline, J.P. Fundamental parameters line profile fitting in laboratory diffractometers. *J. Res. Natl. Inst. Stand. Technol.* **2004**, *109*, 1–25. [CrossRef] [PubMed]
61. Rietveld, H.M. A profile refinement method for nuclear and magnetic structures. *J. Appl. Crystallogr.* **1969**, *2*, 65–71. [CrossRef]
62. Jacobs, H.; Rechenbach, D.; Zachwieja, U. Structure determination of γ'-Fe_4N and ε-Fe_3N. *J. Alloys Compd.* **1995**, *227*, 10–17. [CrossRef]
63. Liapina, T.; Leineweber, A.; Mittemeijer, E.J.; Kockelmann, W. The lattice parameters of epsilon-iron nitrides: Lattice strains due to a varying degree of nitrogen ordering. *Acta Mater.* **2004**, *52*, 173–180. [CrossRef]
64. Niewa, R.; Rau, D.; Wosylus, A.; Meier, K.; Hanfland, M.; Wessel, M.; Dronskowski, R.; Dzivenko, D.A.; Riedel, R.; Schwarz, U. High-Pressure, High-Temperature Single-Crystal Growth, Ab initio Electronic Structure Calculations, and Equation of State of ε-Fe_3N_{1+x}. *Chem. Mater.* **2009**, *21*, 392–398. [CrossRef]
65. Middendorf, C.; Mader, W. Growth and Microstructure of Iron Nitride Layers and Pore Formation in ε-Fe_3N. *Z. Metallkd.* **2003**, *94*, 333–340. [CrossRef]
66. Piller, H. Colour measurements in ore-microscopy. *Miner. Depos.* **1966**, *1*, 175–192. [CrossRef]
67. Atkin, B.P.; Harvey, P.K. The use of quantitative Colour Values for Opaque-Mineral Identification. *Can. Miner.* **1979**, *17*, 639–647.
68. Lei, L.; Yin, W.; Jiang, X.; Lin, S.; He, D. Synthetic Route to Metal Nitrides: High-Pressure Solid-State Metathesis Reaction. *Inorg. Chem.* **2013**, *52*, 13356–13362. [CrossRef]
69. Wriedt, H.A.; Gokcen, N.A.; Nafziger, R.H. The Fe-N (Iron-Nitrogen) system. *Bull. Alloy Phase Diagr.* **1987**, *8*, 355–377. [CrossRef]
70. Caliro, S.; Chiodini, G.; Avino, R.; Minopoli, C.; Bocchino, B. Long time-series of chemical and isotopic compositions of Vesuvius fumaroles: Evidence for deep and shallow processes. *Ann. Geophys.* **2011**, *54*, 137–149. [CrossRef]
71. Balić-Žunić, T.; Garavelli, A.; Jakobsson, S.P.; Jonasson, K.; Katerinopoulos, A.; Kyriakopoulos, K.; Acquafredda, P. Fumarolic Minerals: An Overview of Active European Volcanoes. In *Updates in Volcanology—From Volcano Modelling to Volcano Geology*; Nemeth, K., Ed.; IntechOpen: London, UK, 2016; pp. 267–322. [CrossRef]
72. Chiodini, G.; Marini, L.; Russo, M. Geochemical evidence for the existence of high-temperature hydrothermal brines at Vesuvio volcano, Italy. *Geochim. Cosmochim. Acta* **2001**, *65*, 2129–2147. [CrossRef]
73. Corsaro, R.A.; Cristofolini, R. Origin and differentiation of recent basaltic magmas from Mount Etna. *Miner. Petrol.* **1996**, *57*, 1–21. [CrossRef]
74. Nicotra, E.; Ferlito, C.; Viccaro, M.; Cristofolini, R. Volcanic geology and petrology of the Val Calanna succession (Mt. Etna, Southern Italy): Discovery of a new eruptive center. *Period. Miner.* **2011**, *2*, 287–307. [CrossRef]